ACS APPLIED MATERIALS & INTERFACES

Research Article

www.acsami.org

Large-Area Ordered P-type Si Nanowire Arrays as Photocathode for Highly Efficient Photoelectrochemical Hydrogen Generation

Shufan Huang,[†,∥] Haifeng Zhang,[‡,∥] Zilong Wu,[†] Dezi Kong,[‡] Dongdong Lin,[†] Yongliang Fan,[†] Xinju Yang,[†] Zhenyang Zhong,[†] Shihua Huang,[§] Zuimin Jiang,*[,†] and Chuanwei Cheng*[,‡]

[†]State Key Laboratory of Surface Physics, Key Laboratory of Micro and Nano Photonic Structures (Ministry of Education) and Department of Physics, Fudan University, Shanghai 200433, People's Republic of China

[‡]MOE Key Laboratory of Advanced Micro-structured Materials, School of Physics Science and Engineering, Tongji University, Shanghai 200092, People's Republic of China

[§]Department of Material Physics, Zhejiang Normal University, Jinhua 321004, People's Republic of China

S *Supporting Information*

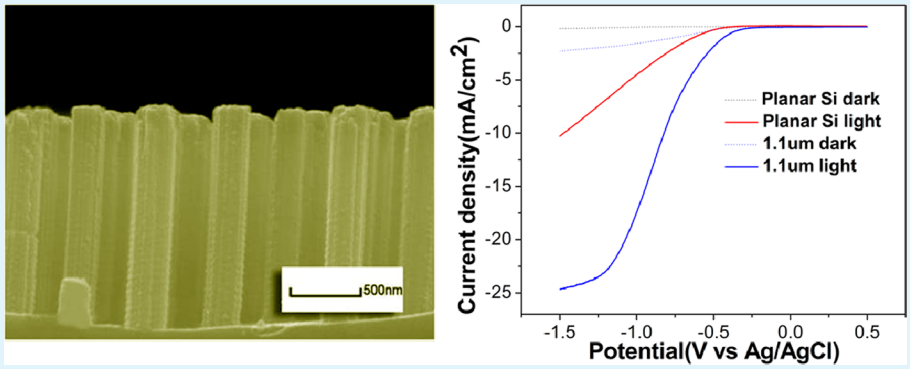

ABSTRACT: In this Article, we report the successful fabrication of large-area ordered Si nanowire arrays (NWAs) by a cost-effective and scalable wet-etching process in combination with nanospheres lithography technique. The periodical Si NWAs are further investigated as photocathode for water splitting, with excellent hydrogen evolution performances with a maximum photocurrent density of 27 mA cm^{-2} achieved, which is ~2.5 times that of planar Si and random Si nanowires electrode. The greatly improved PEC performance can be attributed to the patterned and ordered NWs structure as a result of enhancement of the light harvesting as well as charge transportation and collection efficiency.

KEYWORDS: *large area, ordered array, nanosphere photolithography, Si, PEC*

INTRODUCTION

Continuous concerns on the increasing global energy demand and environmental sustainability have aroused great research interest in developing clean and renewable energy to decrease the reliance on traditional fossil fuels.[1−3]Photoelectrochemical (PEC) water splitting represents a promising approach to harness and store the solar energy into hydrogen fuels.[4−9] To achieve high-efficiency PEC cells is to use dual ligh absorbers, with one as a photocathode, and another acting as a photoanode. In contrast to the deep research on the n-type photoanodes, the development of P-type semiconductors is still far behind. One of the key challenges for PEC devices is developing an efficient photocathode. In general, one ideal photocathode material and configuration should hold the following criteria: First, it has high light harvesting efficiency and low carrier recombination velocity. Second, it should retain a relative high onset potential as far as possible to reduce the reliance on the applied bias. Third, excellent chemical stability is required. In this regard, crystalline Si is an attractive candidate for PEC water splitting due to the eminent physical characteristics, including a narrow band gap (E_g = 1.12 eV) that greatly matches the solar spectrum and the conduction band edge of Si is more negative than the water reduction potential.[10,11] However, there are still some limitations for the application of planar Si in PEC water splitting. One problem is that high light reflectance loss happens on the planar Si−water interface. Another large issue is the poor photostability of Si due to its oxidation in electrolyte. Recent attempts to use nanostructured Si as photocathodes have demonstrated it to be an efficient way to boost the efficiency by enhancing the light absorption and charge collection efficiency.[12−19] In particular, 1D vertical nanowire arrays that decouple the light absorption and charge transportation are an especially attractive electrode design. In the past few years,

Received: February 25, 2014
Accepted: July 14, 2014
Published: July 14, 2014

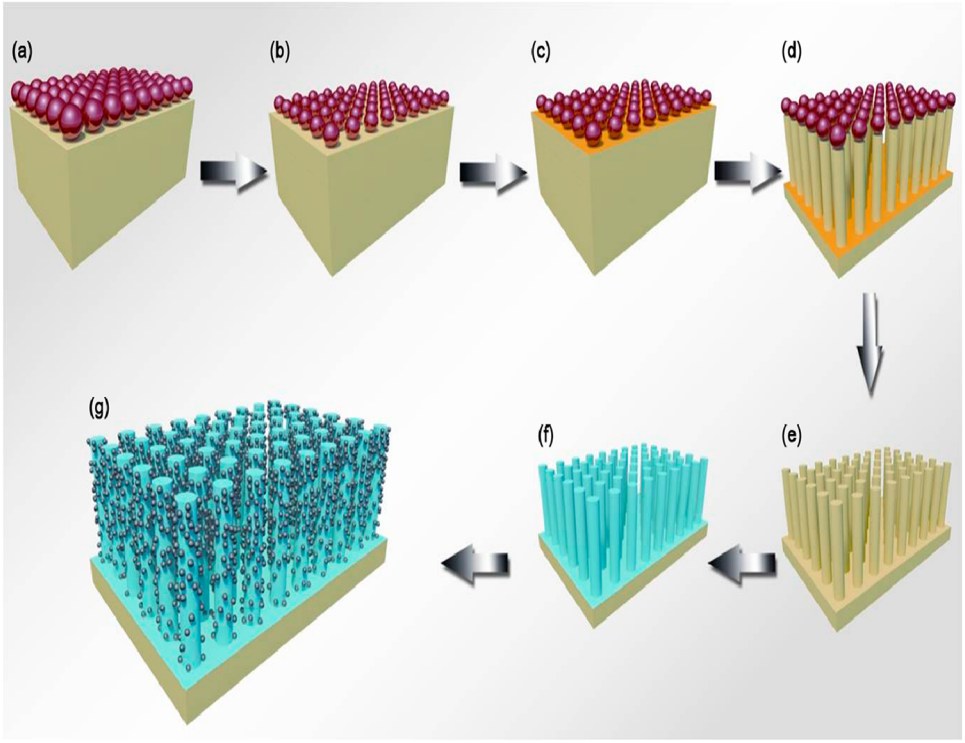

Figure 1. Scheme of the fabrication procedures of Si nanowire arrays with a TiO_2 passivation layer and Pt cocatalyst.

various routes like electroless etching,[20−25] reactive ion dry-etching,[26] and chemical vapor phase growth[27,28] were explored to fabricate vertical aligned Si nanowire electrodes. Among them, the wet-etching method is more promising for its low cost and scalable fabrication process. However, the Si nanowires fabricated by electroless etching were usually very dense and randomly distributed on the wafer, which led to a decrease in light absorption and high surface recombination rates. In this respect, a surface with nanoscale periodic features can offer strong light trapping by creating an optical density gradient from the top surface to the bulk and reduce the charge recombination.[29,30]Moreover, to address the photocorrosion and oxidation issue of Si, a number of materials such as conducting polymers, metallic silicide, and metal oxide have been used to passive the surface. Recent research has demonstrated that thin TiO_2 coating can stabilize the Si surface against oxidation due to the efficient electronic transport through the TiO_2 layer.[10,12] The atomic layer deposition technique allows for fine controlling the thickness of TiO_2 with pinhole free coverage.

Herein, we report a novel photocathode design by using ordered P-type Si nanowires array fabricated by an integration of nanosphere lithography (NSL) and wet-etching process. The NSL technique,[31,32] which uses a monolayer of nanosphere arrays as an etching mask to transfer the patterns into the underlying substrate, is advantageous for preparation of large-area (up to 4-in. wafer) ordered surface patterns within the controllable size in low production cost, as compared to the common e-beam lithography and photolithography tequniques.[16,33−35] The periodical and ordered Si nanowire arrays for photocathodes allow for providing increased surface area, strong light trapping, and direct electron transport paths, leading to enhancement of the light harvesting and charge collection efficiency. When testing them as photocathodes for PEC hydrogen generation, excellent PEC performances with a high photocurrent density of 27 mA cm^{-2} at −1.28 V bias vs RHE and excellent photostability are achieved for Si NWAs in conjuction with a TiO_2 passivation layer and a Pt cocatalyst.

EXPERIMENTAL SECTION

Large-Area Ordered Si NWAs Fabrication. The initial planar Si (MTI, China) wafers were cleaned by a standard RCA method; that is, the substrates were sonicated in DI water, acetone (Sinopharm Chemical Reagent, China), and methanol (Sinopharm Chemical Reagent, China) for 5 min, respectively, followed by a 5 min DI water washing, then bathing in H_2SO_4/H_2O_2 (Sinopharm Chemical Reagent, China) with a volume ratio of 4:1 for 10 min to form a hydrophobic surface; the samples then were washed in DI water for 10 min for the next step use. After that, a monolayer of polystyrene spheres with diameters of 500 nm (Duke Scientific, U.S.) was self-assembled onto the planar Si bulk, the samples were baked at 80 °C for 3 min to remove the residual DI water and other impurities, and before the RIE O_2 treating, the samples were kept in a vacuum environment. The samples were etched by RIE using O_2 gas (Samco, Japan). The gas flow rate was 30 sccm, the power was 30 W, chamber pressure was 74 mTorr, and the etching time was 280 s. Afterward, a 20 nm Au layer was sputtered onto the samples by an ion sputtering apparatus (Cressington, 108Manual, UK) at a constant current of 10 mA; before wet-solution etching, the thickness was monitored by a crystal oscillator. After Au deposition, the samples have to be etched by solution as soon as possible; otherwise, the samples will be polluted. Si nanowire arrays were fabricated by wet etching using HF (Sinopharm Chemical Reagent, China) and H_2O_2 (Sinopharm Chemical Reagent, China) with a volume ratio of 4:1, the etching solution was stirred all of the time, and the length of the nanowire could be adjusted by well controlling the etching time. Finally, the polystyrene spheres were removed by dissolving in toluene, and the remaining Au layer was removed by soaking the sample in KI/I_2 mixed solution (10 g of KI, 2.5 g of I_2, and 100 mL of DI water) for 24 h; after that, the samples were rinsed using DI water and dried with high pure nitrogen. For comparison, the random Si NW was etched as the same procedures except without the nanosphere two-dimensional mask.

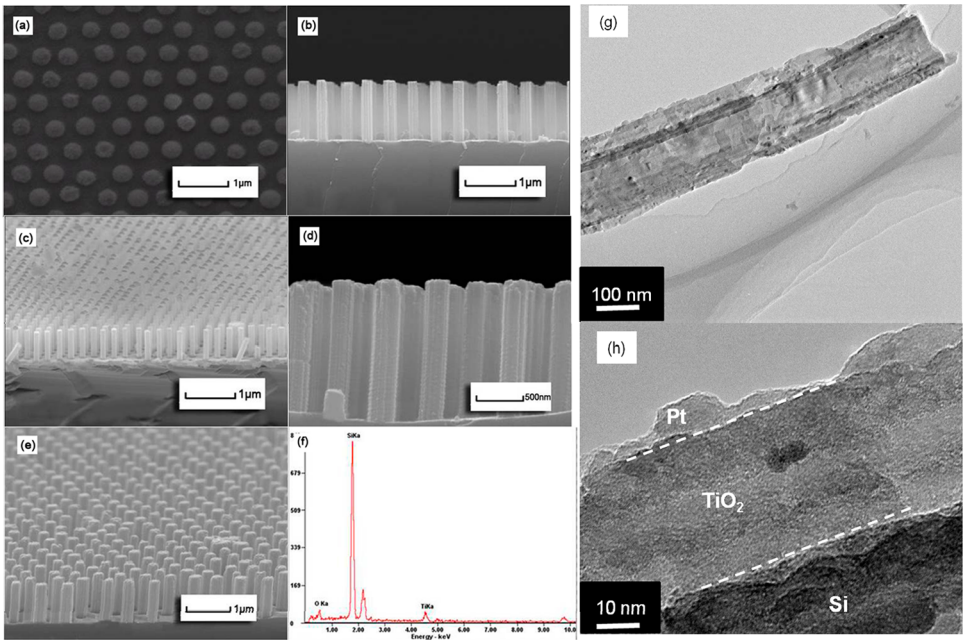

Figure 2. (a) Top-viewed SEM image of PS spheres on the planar Si as an etching mask. SEM images of ordered Si NW arrays: (b) cross-section view; (c) 30 tilted-view and TiO_2-coated Si NW arrays, (d) cross-section view, (e) 30 tilted-view, and (f) EDS spectrum recorded on the surface of TiO_2-coated Si NW arrays. (g) TEM image and (f) HRTEM image of Pt decorated TiO_2/Si nanowire.

Atomic Layer Deposition (ALD) of 30 nm TiO_2. Before the samples were transferred into the ALD chamber, they were dipped in 5% HF solution (Sinopharm Chemical Reagent, China) for 10 min to completely remove the surface oxide layer. A 30 nm TiO_2 passivation layer was deposited by a commercial ALD system (SUNALE R-200) with 208 cycles of $TiCl_4$ (0.3 s pulse) and H_2O (0.3 s pulse). The substrate temperature for TiO_2 growth was kept at 150 °C.

Electron Beam Evaporation of 1 nm Pt. 1−2 nm Pt was deposited onto the TiO_2-coated planar Si and Si/TiO_2 core−shell NWAs by a commercial e-beam evaporation system (Kurt J. Lesker) with a speed of 0.01 nm/S; the thickness of Pt was controlled by a crystal oscillator. The vacuum was kept at 5×10^{-6} Torr during the deposition.

Ohmic Contact Formation of the Samples. 100 nm Al was deposited onto the back side of the samples by e-beam evaporation (Oxford, UK) with a deposition rate of 0.1 nm/s; subsequently, the samples were annealed at 300 °C, for 3 min in forming gas (95% N_2 and 5% H_2) in a homemade rapid thermal annealing oven to form back ohmic contact.

Characterizations. The morphologies of Si NWAs were characterized by a field scanning electron microscopy (FE-SEM, XL30FEG, PHILIPS, Netherlands) equipped with an energy dispersive X-ray spectrometer (EDS) operating at 20 kV. Before SEM tests, a 10 nm Au layer was deposited onto the surface by ion sputtering apparatus (Cressington, 108Manual, UK) at a current of 10 mA to get more distinct figures except for those shown in Supporting Information Figure S4. The element analysis was conducted by the EDS. The hemispherical optical reflectance spectra of planar Si bulk, NWAs samples were collected in a wavelength ranging from 300 to 1100 nm with a step of 5 nm via a UV−vis spectrometer (Zolix, China). Every sample was measured two times, and the results were generally repeated.

Photoelectrochemical Measurements. The PEC measurements of the Si nanowire arrays photocathodes were tested using a CHI760D electrochemical workstation (CHI instrument). Both the PEC and the Mott−Schottky properties measurements of the planar Si, Si nanowire arrays photocathodes were investigated in 0.5 M sulfuric acid (pH ∼0.42) containing a Ag/AgCl reference electrode and a Pt counter electrode under simulated sunlight AM 1.5 (100 mW cm^{-2}) illumination. The stability tests were studied in 0.5 M sulfuric acid (pH ∼0.42) and 1 M sodium hydroxide (pH ∼14.2), respectively. The light source used for simulated sunlight was a 150 W xenon lamp equipped with an air mass 1.5 filter. The incident-photon-to-electron conversion efficiency (IPCE) was collected as a function of wavelength from 300 to 850 nm using a specially designed IPCE system (Zolix Solar cell Scan100), with three electrodes configuration under −0.28 V bias vs RHE. A 150 W Xe lamp and a monochromator equipped with gratings were used to generate a monochromatic beam.

■ RESULTS AND DISCUSSION

The fabrication procedures of large-area ordered Si nanowire arrays are illustrated in Figure 1. First, P-type boron-doped Si wafers (⟨100⟩ oriented, 1−10 and 10−40 Ω cm) cleaned by a standard RCA process were covered with a monolayer of 500 nm closed-packed polystyrene nanosphere (PS) arrays via a self-assembly route, and then the size of the PS spheres was reduced to a specific diameter of about 280 nm as a nanopatterned mask by oxygen plasma etching with a ratio-frequency (RF) power of 30 W. After that, a layer of 20 nm Au film was deposited onto the PS spheres-coated Si substrate serving as an up−down catalysis layer; in a following step, the ordered nanowire arrays were obtained by a general wet-etched process in HF/H_2O_2 mixed solution. The nanowire length can be controlled by adjusting the wet-etching time, while the PS nanosphere patterns defined the diameters and pitches of the nanowires. The remaining Au catalyst layer can be removed by soaking the samples in KI/I_2 solution for 24 h; to stabilize the Si surface, a ∼30 nm thick TiO_2 passivation layer was deposited onto the Si NWAs by ALD at a temperature of 150 °C to improve the chemical stability. Finally, noble metal Pt catalyst with a thickness of 1 nm was sputtered onto the nanowires. For comparison, Si NWs with random alignment were also prepared by a similar process without using the PS sphere as a mask.

Figure 2a shows the SEM image of the PS sphere arrays after oxygen plasma etching, indicating that the PS spheres are assembled in a well-ordered pattern structures. The diameter of each PS sphere is around 280 nm. The typical cross-sectional

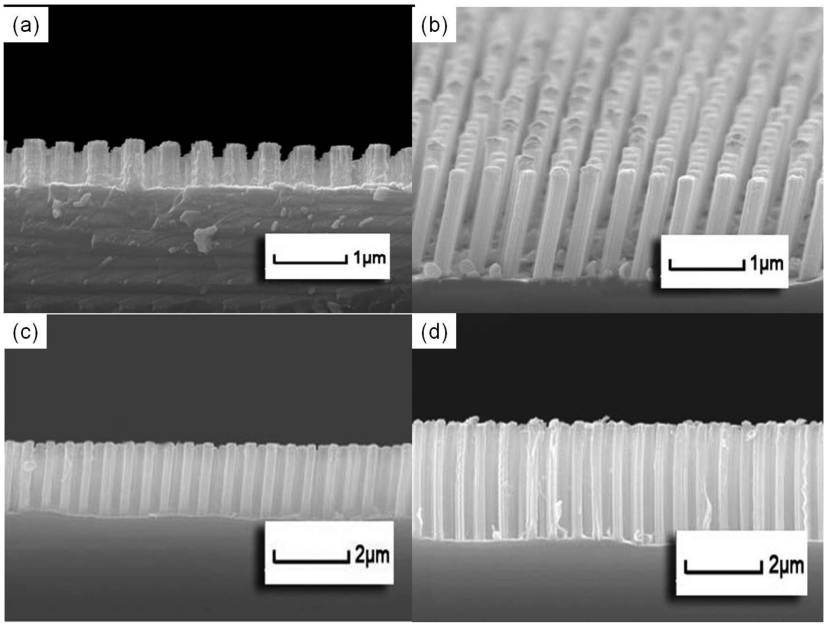

Figure 3. Cross-section SEM images of Si NW arrays with different lengths: (a) 0.6 μm, (b) 1.4 μm, (c) 2.0 μm, (d) 3.1 μm.

and titled-viewed SEM images of Si nanowire arrays with length of 1.1 μm are presented in Figure 2b and c, respectively. It can be observed that the Si nanowires are vertically aligned on the substrate with well periodical structures in a large-scale area. The diameters and adjacent distances of the Si nanowires are around 250 and 300 nm, respectively. Without the use of PS spheres, dense and randomly aligned Si nanowires were obtained, as displayed in Supporting Information Figure S1. After the ALD coating of TiO_2, the morphology of the Si nanowire arrays did not change much except for a little increase in the diameters as depicted in Figure 2d and e. The EDS measurement taken from the TiO_2-coated Si nanowires confirms the chemical composition of Si and TiO_2. According to the SEM, it can be roughly estimated that the surface area of the NWAs can be increased an order of magnitude as compared to that of planar Si bulk. The TEM and HRTEM image observations of Pt decorated TiO_2/Si nanowire in Figure 2g and h further confirm that the Si nanowire is successfully covered with ~30 nm of TiO_2 and ~1−2 nm of Pt. As indicated in Figure 3, the length of the ordered Si nanowires can be finely controlled to range from 0.6 to 3.1 μm by adjusting the etching times.

To investigate the antireflection properties of the Si NWAs, the total hemispherical optical reflectance spectra of planar Si bulk and ordered Si NWAs with different lengths in a wavelength range of 300−1100 nm were measured. As shown in Figure 4, it is evident that the large-scale ordered bare Si NWAs drastically suppress the reflection across the whole measured spectrum with wavelength above Si band gap (1.12 eV) as compared to that of planar Si wafer. We note that the ordered Si nanowire arrays provide better light trapping ability than that of the random one in the wavelength region of 300−800 nm. Moreover, the optical reflectance intensity decreases with the length of the Si NW increase, which is consistent with previous reports about random Si NWAs by electroless etching.[20,21] The superior antireflection properties of the Si NWAs can be attributed to the increased surface area as well as the well-ordered plus periodical structures that enable strong light trapping and scattering, as a result of increasing the light

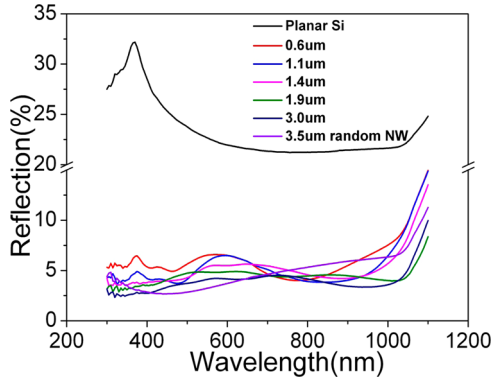

Figure 4. Total hemispherical optical reflectance of planar Si bulk, random Si NW arrays, and large-area ordered bare Si NW arrays with different lengths ranging from 0.6 to 3.1 μm.

harvesting. We note that the deposition of TiO_2 or Pt onto the Si NWAs does not increase the reflectance, as demonstrated in Supporting Information Figure S3, while for the Pt-coated planar Si control, the reflectance intensity is increased due to the strong light reflection ability of the Pt metal particles.

To study the photoelectrochemical water splitting performance, the photocurrent density versus potential curves are measured in the dark and under AM1.5 (100 mW cm^{-2}) simulated sunlight illumination by using the ordered Si NWAs and planar Si as photocathode. The electrochemical tests are conducted in a typical three-electrode configuration with the Si NWAs as working electrode, one Ag/AgCl (saturated KCl) as the reference electrode, and a Pt plate as the counter electrode. Figure 5a depicts the typical $J-V$ curves of the Si NWAs with 1.1 μm length, Si random NW arrays, and planar Si electrodes. In the dark, the photocurrent is very small. Under light illumination, obvious photocurrent density is observed for both planar Si and Si NWAs electrodes, indicating efficient charge generation and separation in the semiconductor/liquid junctions. As shown in Figure 5a, the photocurrent density of Si NWAs electrode gradually increases due to the potential of 0.05 V vs RHE and approaches a maximum value of −25 mA

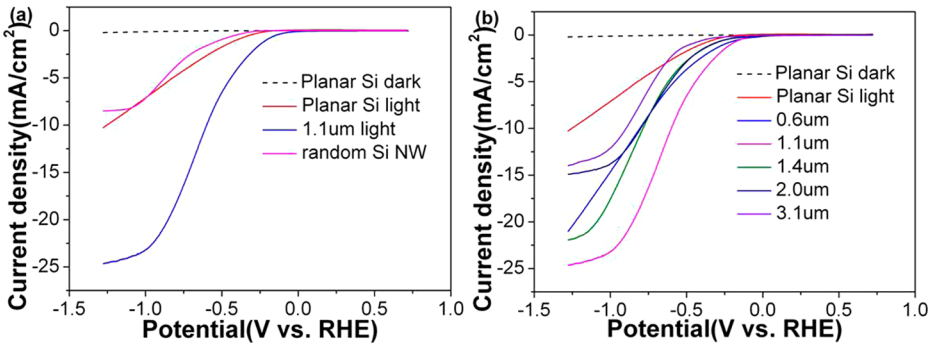

Figure 5. Photocurrent density versus applied potential curves of (a) TiO_2-coated planar Si and 1.1 μm ordered Si/TiO_2 core−shell NW arrays, and (b) ordered Si/TiO_2 core−shell NW arrays with different lengths.

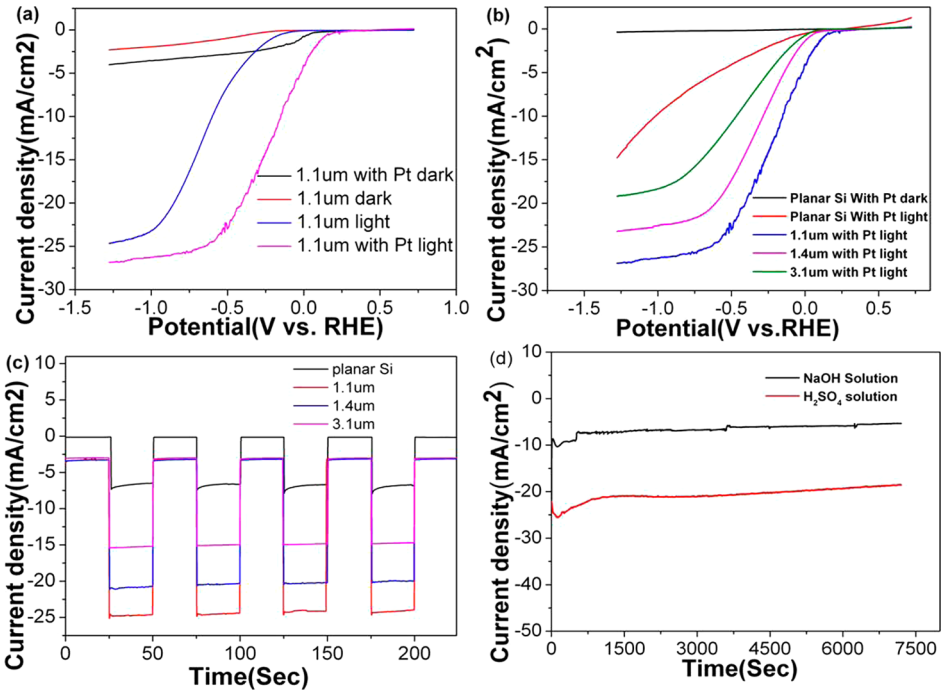

Figure 6. Photocurrent density versus applied potential curves of (a) ordered Si/TiO_2 and Pt decorated Si/TiO_2 core−shell NWs, and (b) Pt decorated planar Si and ordered Si/TiO_2 core−shell NWs with different lengths measured in the dark and under 100 mW cm^{-2} illumination. (c) Amperometric i−t curves for Pt decorated planar and ordered Si/TiO_2 core−shell NWs with different lengths. (d) Stability test of 1.1 μm Pt decorated Si/TiO_2 core−shell NW arrays in electrolyte solution for 2 h under 100 mW cm^{-2} illumination.

cm^{-2} at −1.28 V vs RHE, which is about 2.5 times higher than that of planar Si and random Si NW arrays. Moreover, the onset potential of Si NWAs electrode is ∼0.05 V vs RHE, and anodically shifts around 0.2 V, in contrast to that of planar Si electrode (−0.15 V vs RHE). This might be due to the catalytic effect induced by the residual Au nanoparticles adhering to the surface of the Si NWAs.[8] The greatly improved PEC performance for the Si NWAs can be attributed to the following reasons. First, the NWs structures greatly increase the surface area, enabling one to enhance the light absorption; moreover, the well-ordered periodical NWAs greatly enhance the light trapping and scattering, as a result of enhancing the light harvesting. Second, the vertical 1D NWs that decouple the light absorption and charge transportation are able to reduce the minority carrier diffusion length and enhance the charge transportation and collection efficiency. Importantly, the patterned and ordered structures are beneficial to reduce the charge recombination loss in comparison to that of random nanowires. Third, the increased elecrode/elecrolyte contact area can provide more reaction sites and reduce the overpotential for H_2 generation. We note that the dark current density for the Si NWAs electrode is also increased, which might be due to the higher surface recombination velocity that arises from the increased surface area. The effect of the length of Si NWs on the PEC performance was also investigated. As shown in Figure 5b, the photocurrent density of the Si NWs electrode first increases with the length and approaches a maximum value at the length of 1.1 μm; it then decreases with the further longer length. This is because there is a trade-off between the surface area and recombination loss. In other words, with the length increase, the total surface area increases, as a result of enhancement of the light absorption, while the surface recombination will also increase, and this would decrease the photocurrent density. So the optimal length of Si NWs in this case is ∼1.1 μm. Moreover, the doping level of Si NWAs also plays an important role on the PEC performance. Two different Si wafers with resistivities of 1−10 and 10−40 Ω cm were used as the substrates for preparation of Si NWAs; the

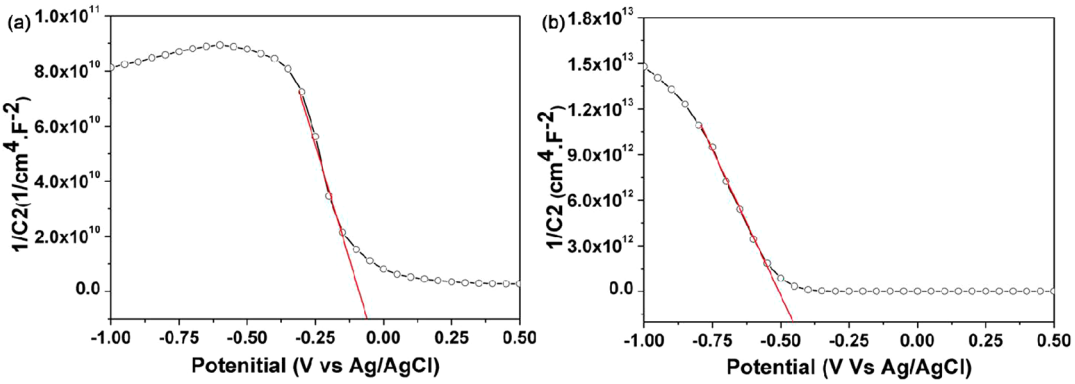

Figure 7. Mott–Schottky measurements of (a) TiO_2-coated planar Si and (b) 1.1 μm large-area ordered Si/TiO_2 core–shell NW array.

cross-section and titled-viewed SEM images are shown in Supporting Information Figure S6a and b. Supporting Information Figure S6c compares the $J-V$ curves of the two different doping NWAs electrodes; it is found that the Si NWAs electrode with higher doping level possesses better PEC performance, implying more efficient charge generation and collection.

To further anodically shift the onset potential, ~1 nm Pt nanoparticles were deposited onto the Si NWAs surface. Figure 6a presents the comparison of $J-V$ curves of the Si NWAs electrode with and without Pt catalyst. The onset potential is remarkably positively shifted 180 mV for the Pt decorated Si NWAs, and the photocurrent density is also slightly increased from 25 to 27 mA cm^{-2} due to the electrocatalytic effect of Pt, which is arising from the good dispersion of Pt nanoparticles on the ordered Si NWs surface, in contrast to the previous reports on Pt decorated chemical-etched randoms Si NWs.[36,37]

A similar tendency on the relationship between the NWAs length and photocurrent density is also observed in the Pt-coated Si NWAs samples, as indicated in Figure 6b. The transient current density versus time curves of Pt decorated Si NWAs and planar Si electrodes (Figure 6c) measured under chopped illumination at −0.78 V vs RHE display fast light response and excellent switching performance.

Another important issue for the PEC devices application is the chemical stability of the photoelectrode. Figure 6d shows the $i-t$ curve of the Pt decorated Si NWAs with TiO_2 surface passivation measured under 100 mW cm^{-2} simulated solar light illuminations with a period of 2 h at a bias of −0.78 V vs RHE in both 0.5 M sulfuric acid (pH ~0.42) and 1 M NaOH (pH ~14.2) electrolyte, respectively. It is clear that the electrode presents excellent chemical stability in both acid and base electrolytes with good photocurrent retention ability. The cross-section and tilted-viewed SEMs of the sample after 2 h stability test shown in Supporting Information Figure S5c and d demonstrate the NWAs still keep the ordered structure without any damage.

The photoactivity of Si NWAs photocathode as a function of wavelength was also quantatively evaluated by measuring the IPCE spectra.The IPCE was caculated by measuring the photocurrent at different wavelengths at a bias −0.28 V vs RHE. As shown in Supporting Information Figure S7, the Si NWAs photocathode shows 25–30% of IPCE values in the entire visible wavelength range of 300–850 nm.

To investigate the electronic property, for example, flat band potential and carrier concentration of the Si NWAs, electrochemical impedance measurements were conducted. Figure 7a and b shows that both of the planar Si and Si NWAs samples have a negative slope in the Mott–Schottky plots, suggesting the P-type semiconductor feature of Si. In contrast to the planar Si, the flat-band potential of Si NWAs electrode cathodically shifts from −0.17 to −0.23 V vs RHE, corresponding to the increased surface band bending. Besides, the carrier densities can be obtained from the slopes of Mott–Schottky plots using the following equation:

$$N_d = (2/e_0\varepsilon\varepsilon_o)[d/C^2/dV]^{-1}$$

where e_0 is the electron charge, ε is the dielectric constant of Si, ε_0 is the permittivity of vacuum, N_d is the carrier density, and V is the applied bias across the electrode. As compared to planar Si, the Si NWAs have a smaller slope, which indicates slightly increased carrier densities induced by the surface defects.

CONCLUSION

In summary, we have fabricated large-area ordered Si nanowire arrays by a cost-effective and scalable wet-etching process in combination with nanosphere lithography technique. The periodical Si NWAs drastically suppressed the light reflectance by strong light scattering and trapping effect. For PEC water splitting application, a maximum photocurrent density of 27 mA cm^{-2} is obtained by using Pt decorated Si NWAs with length of 1.1 μm as photocathode, which was 2.5 times higher that of planar Si electrode. Besides, the Si NWAs electrode presents excellent chemical stability by TiO_2 passivation. The greatly improved PEC performance can be attributed to patterned and ordered NWs structure as a result of increasing surface area and enhancement of light harvesting as well as improvement in charge transportation and collection efficiency. The cost-effective and scalable method for large-area Si NWAs opens an opportunity for developing high efficiency and low-cost PEC devices.

ASSOCIATED CONTENT

Supporting Information

SEM images, optical refletance spectrum, AFM images, and $J-V$ curves of the planar Si and Si nanowire. This material is available free of charge via the Internet at http://pubs.acs.org.

AUTHOR INFORMATION

Corresponding Authors

*E-mail: zmjiang@fudan.edu.cn.
*E-mail: cwcheng@tongji.edu.cn.

Author Contributions

[‖]These authors contributed equally.

Notes

The authors declare no competing financial interest.

■ ACKNOWLEDGMENTS

This work was financially supported by 973 Program (Grant nos. 2011CB925601 and 2013CB632701), the National Natural Science Foundation of China (Grant nos. 51202163, 61076055), the Shanghai Pujiang Program (Grant no. 12PJ1408200), the Innovation Program of Shanghai Municipal Education Commission (Grant no. 13ZZ025), and the Fundamental Research Fund for Central University.

■ REFERENCES

(1) Potocnik, J. Renewable Energy Sources and the Realities of Setting an Energy Agenda. *Science* **2007**, *315*, 810−811.
(2) Lewis, N. S.; Nocera, D. G. Powering the Planet: Chemical Challenges in Solar Energy Utilization. *Proc. Natl. Acad. Sci. U.S.A.* **2006**, *103*, 15729−15735.
(3) Gratzel, M. Photoelectrochemical Cells. *Nature* **2001**, *414*, 338−344.
(4) Turner, J. A. A Realizable Renewable Energy Future. *Science* **2004**, 972−974.
(5) Tachibana, Y.; Vayssieres, L.; Durrant, J. R. Artificial Photosynthesis for Solar Water Splitting. *Nat. Photonics* **2012**, *6*, 511−518.
(6) Chen, X. B.; Guo, L. J.; Samuel, S. M. Semiconductor-based Photocatalytic Hydrogen Generation. *Chem. Rev.* **2010**, *110*, 6503−6570.
(7) Noh, S. Y.; Sun, K.; Choi, C. L.; Niu, M. T.; Yang, M. C.; Xu, K.; Jin, S. h.; D. L. Wang, D. L. Branched TiO_2/Si Nanostructures for Enhanced Photoelectrochemical Water Splitting. *Nano Energy* **2013**, *2*, 351−360.
(8) Oh, J.; Deutsch, T. G.; Yuan, H. C.; Branz, H. M. Nanoporous Black Silicon Photocathode for H_2 Production by Photoelectrochemical Water Splitting. *Energy Environ. Sci.* **2011**, *4*, 1690−1694.
(9) Cheng, C. W.; Zhang, H. F.; Ren, W. N.; Dong, W. J.; Sun, Y. Three Dimensional Urchin-like Ordered Hollow TiO_2/ZnO Nanorods Structure as Efficient Photoelectrochemical Anode. *Nano Energy* **2013**, *2*, 779−786.
(10) Chen, Y. W.; Prange, J. D.; Duhnen, S.; Park, Y.; Gunji, M.; Chidsey, C. D.; Mclntyre, P. Atomic Layer-Deposited Tunnel Oxide Stabilizes Silicon Photoanodes for Water Oxidation. *Nat. Mater.* **2011**, *10*, 539−544.
(11) Dai, P. C.; Xie, J.; Mayer, M. T.; Yang, X. G.; Zhan, J. H.; Wang, D. W. Solar Hydrogen Generation by Si Nanowires with Atomic Layer Deposition Pt Nanoparticle Catalysts. *Angew. Chem., Int. Ed.* **2013**, *52*, 11119−11123.
(12) Hwang, Y. J.; Boukai, A.; Yang, P. D. High Density n-Si/TiO_2 Core/Shell Nanowire Arrays with Enhanced Photoactivity. *Nano Lett.* **2009**, *9*, 410−415.
(13) Boettcher, S. W.; Warren, E. L.; Putnam, M. C.; Santori, E. A.; Evans, D. T.; Kelzenberg, M. D.; Walter, M. G.; McKone, J. R.; Brunschwig, B. S.; Atwater, H. A.; Lewis, N. S. Photoelectrochemical Hydrogen Evolution Using Si Microwire Arrays. *J. Am. Chem. Soc.* **2011**, *133*, 1216−1219.
(14) Hwang, Y. J.; Wu, C. H.; Hahn, C.; Jeong, H. E.; Yang, P. D. Si/InGaN Core/Shell Hierarchical Nanowire Arrays for Solar Water Splitting. *Nano Lett.* **2012**, *12*, 1678−1682.
(15) Liu, R.; Stephani, C.; Han, J. J.; Tan, K. L.; Wang, D. W. Silicon Nanowires Show Improved Performance as Photocathode for Catalyzed Carbon Dioxide Photofixation. *Angew. Chem., Int. Ed.* **2013**, *52*, 4225−4228.
(16) Zhang, Y.; Wang, H.; Liu, Z.; Zou, B.; Duan, C. Y.; Yang, T.; Yang, X. J.; Zheng, C. J.; Zhang, X. H. Optical Absorption and Photoelectrochemical Performance Enhancement in Si Tube Array for Solar Energy Harvesting Application. *Appl. Phys. Lett.* **2013**, *102*, 163906−163908.
(17) Warren, E. L.; McKone, J. R.; Atwater, H. A.; Gray, H. B.; Lewis, N. S. Hydrogen-Evolution Characteristics of Ni-Mo-Coated, Radial Junction, n(+)p-Silicon Microwire Array Photocathodes. *Energy Environ. Sci.* **2012**, *5*, 9653−9661.
(18) Kelzenberg, M. D.; Turner-Evans, D. B.; Kayes, B. M.; Filler, M. A.; Putnam, M. C.; Lewis, N. S.; Atwater, H. A. Photovoltaic Measurements in Single-Nanowire Silicon Solar cells. *Nano Lett.* **2008**, *8*, 710−714.
(19) McKone, J. R.; Warren, E. L.; Bierman, M. J.; Boettcher, S. W.; Brunschwig, B. S.; Lewis, N. S.; Gray, H. B. Evaluation of Pt, Ni, and Ni-Mo Electrocatalysts for Hydrogen Evolution on Crystalline Si Electrodes. *Energy Environ. Sci.* **2011**, *4*, 3573−3583.
(20) Peng, K. Q.; Huang, Z. P.; Zhu, J. Fabrication of Large-Area Silicon Nanowire P-N Junction Diode Arrays. *Adv. Mater.* **2004**, *16*, 73−76.
(21) Huang, Z. P.; Fan, H.; Zhu, J. Fabrication of Silicon Nanowire Arrays with Controlled Diameter, Length, and Density. *Adv. Mater.* **2007**, *19*, 744−748.
(22) Jung, J. Y.; Choi, M. J.; Zhou, K. Y.; Li, X. P.; Jee, S. W.; Um, H. D.; Park, M. J.; Park, K. T.; Bang, J. H.; Lee, J. H. Photoelectrochemical Water Splitting Employing a Tapered Silicon Nanohole Array. *J. Mater. Chem. A* **2014**, *2*, 833−842.
(23) Shi, J.; Hara, Y.; Sun, C. L.; Anderson, M. A.; Wang, X. D. Three-dimensional High-Density Hierarchical Nanowire Architecture for High-Performance Photoelectrochemical Electrodes. *Nano Lett.* **2011**, *11*, 3413−3419.
(24) Peng, K. Q.; Wang, X.; Lee, S. T. Silicon Nanowire Array Photoelectrochemical Solar Cells. *Appl. Phys. Lett.* **2008**, *92*, 163103.
(25) Wang, X.; Peng, K. Q.; Pan, X. J.; Chen, X.; Yang, Y.; Li, L.; Meng, X. M.; Zhang, W. J.; Lee, S. T. High-Performance Silicon Nanowire Array Photoelectrochemical Solar Cells Through Surface Passivation and Modification. *Angew. Chem., Int. Ed.* **2011**, *50*, 9861−9865.
(26) Geyer, N.; Huang, Z. P.; Fuhrmann, B.; Grimm, S.; Reiche, M.; Nguyen, T. K.; Boor, J. D.; Leipner, H. S.; Werner, P.; Goesele, U. Sub-20 nm Si/Ge Superlattice Nanowires by Metal-Assisted etching. *Nano Lett.* **2009**, *9*, 3106−3110.
(27) Bottcher, S. W.; Spurgeon, J. M.; Putnam, M. C.; Warren, E. L.; Turner-Evans, D. B.; Kelzenberg, M. D.; Maiolo, J. R.; Atwater, H. A.; Lewis, N. S. Energy-Conversion Properties of Vapor-Liquid-Solid-Grown Silicon Wire-Array Photocathodes. *Science* **2010**, *327*, 185−187.
(28) Santori, E. A.; Maiolo, J. R.; Bierman, M. J.; Strandwitz, N. C.; Kelzenberg, M. D.; Brunschwig, B. S.; Atwater, H. A.; Lewis, N. S. Photoanodic Behavior of Vapor-Liquid-Solid-Grown, Lightly Doped, Crystalline Si Microwire Arrays. *Energy Environ. Sci.* **2012**, *5*, 6867−6871.
(29) Kelzenberg, M. D.; Boettcher, S. W.; Putnam, J. A.; Warren, E. L.; Spurgeon, J. M.; Briggs, R. M.; Lewis, N. S.; Atwater, H. A. Enhanced Absorption and Carrier Collection in Si Wire Arrays for Photovoltaic Applications. *Nat. Mater.* **2010**, *9*, 239−244.
(30) Li, J. S.; Yu, H. Y.; Wong, S. M.; Zhang, G.; Sun, X. W.; Qiang Lo, P. G.; Kwong, D.-L. Si Nanopillar Array Optimization on Si Thin Films for Solar Energy Harvesting. *Appl. Phys. Lett.* **2009**, *95*, 033102.
(31) Chen, P. X.; Fan, Y. L.; Zhong, Z. Y. Fabrication and Application of Patterned Si (001) Substrates with Ordered Pits via Nanosphere Lithography. *Nanotechnology* **2009**, *20*, 095303−095308.
(32) Ma, Y. J.; Zhong, Z. Y.; Lv, Q.; Zhou, T.; Yang, X. J.; Fan, Y. L.; Wu, Y. Q.; Zou, J.; Jiang, Z. M. Formation of Coupled Three-Dimensional GeSi Quantum Dot Crystals. *Appl. Phys. Lett.* **2012**, *100*, 153113.
(33) Kargar, A.; Sun, K.; Jing, Y.; Choi, C.; Jeong, H. S.; Zhou, Y. C.; Madsen, K.; Naughton, P.; Jin, S. H.; Jung, G. Y.; Wang, D. L. Tailoring n-ZnO/p-Si Branched Nanowire Heterostructures for Selective Photoelectrochemical Water Oxidation or Reduction. *Nano Lett.* **2013**, *13*, 3017−3022.

(34) Kargar, A.; Sun, K.; Kim, S. J.; Lu, D. L.; Jing, Y.; Liu, Z. W.; Pan, X. Q.; Wang, D. L.Three-Dimensional ZnO/Si Broom-like Nanowire Heterostructures as Photoelectrochemical anodes for Solar Energy Conversion. *Phys. Status Solidi A* **2013**, *210*, 2561−2568.
(35) Sun, K.; Jing, Y.; Li, C.; Zhang, X. F.; Aguinaldo, R.; Kargar, A.; Madsen, K.; Banu, K.; Zhou, Y. C.; Bando, Y. S.; Liu, Z. W.; Wang, D. L. 3D Branched Nanowire Heterojunction Photoelectrodes for High-Efficiency Solar Water Splitting and H_2 Generation. *Nanoscale* **2012**, *4*, 1515−152.
(36) Oh, I.; Kye, J.; Hwang, S. Enhanced Photoelectrochemical Hydrogen Production From Silicon Nanowire Array Photocathode. *Nano Lett.* **2012**, *12*, 298−302.
(37) Sim, U.; Jeong, H.-Y.; Yang, T.-Y.; Nam, K. T. Nanostructural Dependence of Hydrogen Production in Silicon Photocathodes. *J. Mater. Chem. A* **2013**, *1*, 5414−5422.